INTERNATIONAL JOURNAL OF CHEMICAL REACTOR ENGINEERING

Volume 6 2008 *Article* A28

Spatiotemporal Compound Wavelet Matrix Framework for Multiscale/Multiphysics Reactor Simulation: Case Study of a Heterogeneous Reaction/Diffusion System

Sudib K. Mishra[*] Krishna Muralidharan[†] S. Pannala[‡]
Srdjan Simunovic[**] C. Stuart Daw[††] Phani Nukala[‡‡]
Rodney Fox[§] Pierre A. Deymier[¶] George N. Frantziskonis[‖]

[*]University of Arizona, sudib@email.arizona.edu
[†]University of Arizona, krishna@email.arizona.edu
[‡]Oak Ridge National Laboratory, pannalas@ornl.gov
[**]Oak Ridge National Laboratory, simunovics@ornl.gov
[††]Oak Ridge National Laboratory, dawcs@ornl.gov
[‡‡]Oak Ridge National Laboratory, nukalapk@ornl.gov
[§]Iowa State University, rofox@iastate.edu
[¶]University of Arizona, deymier@email.arizona.edu
[‖]University of Arizona, frantzis@email.arizona.edu

ISSN 1542-6580

Spatiotemporal Compound Wavelet Matrix Framework for Multiscale/Multiphysics Reactor Simulation: Case Study of a Heterogeneous Reaction/Diffusion System*

Sudib K. Mishra, Krishna Muralidharan, S. Pannala, Srdjan Simunovic, C. Stuart Daw, Phani Nukala, Rodney Fox, Pierre A. Deymier, and George N. Frantziskonis

Abstract

We present a mathematical method for efficiently compounding information from different models of species diffusion from a chemically reactive boundary. The proposed method is intended to serve as a key component of a multiscale/multiphysics framework for heterogeneous chemically reacting processes. An essential feature of the method is the merging of wavelet representations of the different models and their corresponding time and length scales. Up-and-down-scaling of the information between the scales is accomplished by application of a compounding wavelet operator, which is assembled by establishing limited overlap in scales between the models. We show that the computational efficiency gain and potential error associated with the method depend on the extent of scale overlap and wavelet filtering used. We demonstrate the method for an example problem involving a two-dimensional chemically reactive boundary and first order reactions involving two species.

KEYWORDS: multiscale, multiphysics, wavelets, reaction, diffusion

---

*This research is sponsored by the Mathematical, Information, and Computational Sciences Division; Office of Advanced Scientific Computing Research; U.S. Department of Energy with Dr. Anil Deane as the program manager. The work was partly performed at the Oak Ridge National Laboratory, which is managed by UT-Battelle, LLC under Contract No. De-AC05-00OR22725. Discussions with M. Syamlal, T. J. O'Brien, and D. Alfonso of the National Energy Technology Laboratory (NETL), Stuart Daw of Oak Ridge National Laboratory, and Rodney Fox and Z. Gao of Iowa State University have been very useful.

1. Introduction and Background

A demanding challenge in many branches of physical sciences is to bridge relevant length and time scales as *seamlessly* as possible. Of particular interest in reaction engineering is the accurate simulation of heterogeneous reaction processes such as fluid catalytic cracking (FCC), polymerization, and coal/biomass gasification where the micro-scale processes at the phase interfaces must be accurately resolved. Such high resolution is needed when the details of the microscopic processes (e.g., the nano-scale solid surface topology) control the global reaction and diffusion rates at the mesoscopic scales.

Microscopic and mesoscopic interactions typically manifest themselves as closure relationships for drag, heat and mass transfer in continuum level simulations. There has been significant work in recent years in applying the Lattice Boltzmann method to particle ensembles to derive drag correlations [Hill et al., 2001a and 2001b; van der Hoef et al., 2005], and these new simulation-based correlations have been a valuable addition to existing experiment-based correlation in improving the accuracy of the hydrodynamic gas-solid flows. However, most continuum simulations still employ experiment-based correlations for heat and mass transfer for heterogeneous reacting flows. Often the time and spatial length scales associated with different correlations in the literature can vary by several orders of magnitude [Breault, 2007], and this inconsistency can seriously hamper the accuracy of the large scale simulations employing these correlations. In addition, surface modifications over time (e.g., due to phase changes or sintering) can drastically alter the nature of the inter-phase coupling processes. Thus the development of computational approaches for directly addressing the details of inter-phase physics is highly desirable if significant gains in simulation accuracy are ever to be achieved.

Before applying any new algorithms and techniques to a complicated chemical reactor, one can conceive of a basic building-block which mimics the heterogeneous reactive flow over a catalytic surface. This prototype problem is a multi-scale, multi-physics problem involving four distinct physical processes (Fig. 1): Fluid motion (F), Reactant Species Transport (T), Fluid-Wall Interaction (W), and Wall Chemical Reactions (C). Each process involves characteristic time and length scales that evolve with local thermodynamic and chemical conditions. Generally speaking, processes F and T can be considered to be macroscopic, W is intermediate, and C has microscopic character and chemical-reaction dependent time-scales. The relevant F time scales are the advective and momentum-diffusion times, while T time scale is related to mass-diffusion time of the species. W and especially C processes are at the time step of chemical wall transfer and chemical reaction on the substrate, which are several orders of magnitudes smaller than the

former two. In order to simulate macroscopic devices, both temporal and spatial scaling is necessary.

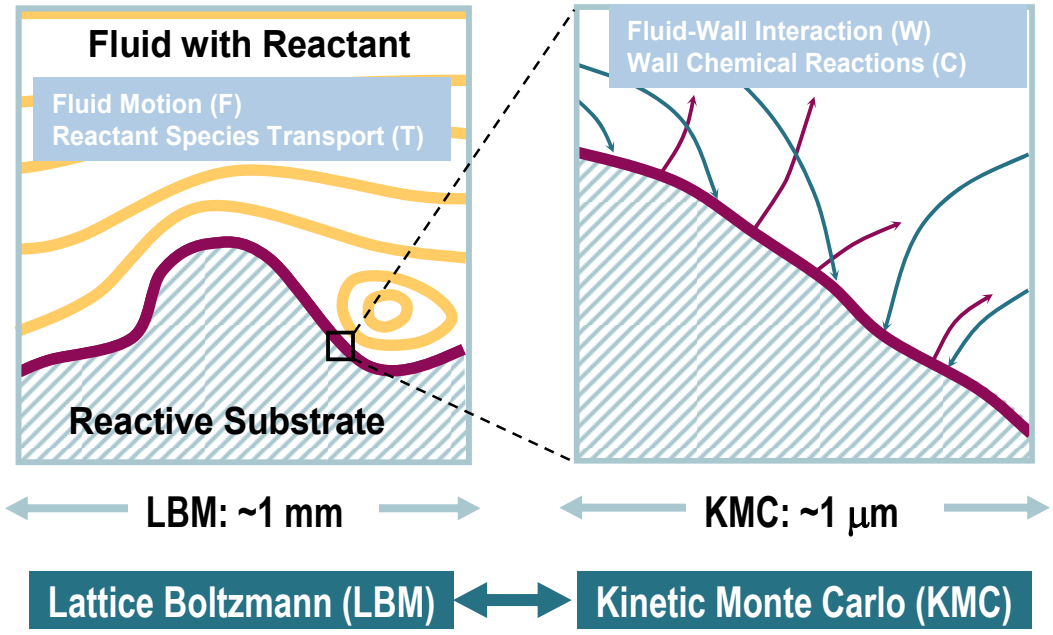

Fig. 1 Illustration of the combined multiscale Lattice Boltzmann Method (LBM)/Kinetic Monte Carlo (KMC) scheme. In the LBM regime, the system length scale is ~ 1 mm, and the description is in terms of hydrodynamic fluid flows (gold lines). In the KMC regime the scale of the cell is ~ 1 μm, and the description is in terms of fluxes of reactants (green arrows) and reaction products (red arrows) determined by the diffusion, advection and chemical reactivity rates (Adapted from [Succi et al, 2001]).

The challenge in multi-scale simulation is to bridge (as seamlessly as possible) the appropriate physical length and time scales, while keeping the computational problem within tractable limits. Although in principle a complete macroscopic simulation can be built up by fully accounting for all of the microscopic processes, the practical futility of such an approach is obvious when the macro- and micro-scales dominating the physics are many orders of magnitude apart. This can be clearly seen for problems where both KMC and LBM type physics are important. The typical time-steps encountered in KMC simulations are of the order of nano- to micro-seconds; where as the spatial extent can vary from nano- to micro-meters depending on the resolution of the solution space and the processes resolved. However, the typical time-steps in LBM

simulations vary from micro- to millisecond while the spatial resolution varies from micro- to millimeter. It is an obvious challenge to couple the physics at these two scales which vary over six orders magnitude in both space and time.

For heterogeneous reactive flows, we propose to implement a specific type of Hierarchical Multiscale Modeling (HMM), which provides up- and down-scaling between the relevant processes (at their respective length and time scales) without the need for full simulations at the microscopic levels. We apply our approach to couple the mesoscale LBM, which is suitable for modeling multiphase reacting flows with low Mach numbers, and the microscale KMC for modeling of chemical reactions on catalytic surfaces. Projections and reductions between these two types of models are primarily sought by a space- and time-based CWM. We believe this coupling method constitutes a new paradigm for modeling multi-scale reaction systems and addresses the need for more efficient and accurate simulations in a unique way.

In this paper, we simplify the above prototype problem further and consider mass transport only by diffusion to demonstrate the underlying coupling algorithm. At microscopic time and length scales, we employ kinetic Monte Carlo (KMC) to simulate kinetics of chemical reactions. Diffusion away from the reactive boundary operates on mesoscopic scales and we employ finite-difference of the diffusion equations. Direct coupling of the two models is computationally and conceptually impractical for realistic scenarios. For example, the time integration in coupled simulations is controlled by the KMC, thus prohibiting simulation over practical temporal and spatial (diffusion) scales. However, the KMC/diffusion simulations, in the following termed as the "*fine*" model, would provide information not only on the mean response of the system but also on its fluctuations, which is important for the robust understanding of these reaction/diffusion kinetics. In contrast to the *fine* model, deterministic modeling of the reactions combined with coarse-grained continuum-based modeling of the diffusion provide a model, termed "*coarse*" trades off the resolution with the ability to model much larger time increments and spatial domains.

Both models are limited in either resolution or length of time over which simulations can be run, thus it is desirable to compound the two models by extracting the most useful and relevant information from each. Such a compounding process provides an avenue for approaching the complete behavior and can be greatly facilitated by the use of the wavelet transform, which allows for a natural decomposition of information in (spatial or temporal) scales. The compound wavelet matrix technique (CWM) [Frantziskonis et al, 2006 and references therein] can spatially as well as temporally decompose both the *fine* and *coarse* simulations by using the forward wavelet transform for each, compound the information by forming a "union" CWM, and then, if needed, perform the inverse (backward) wavelet transform to obtain the spatiotemporal

information on the reaction/diffusion problem for long time periods and large spatial domains without considerable loss of information. In short, the CWM aims at using the computational efficiency of the *coarse* model yet retaining the accuracy of the *fine* one by compounding the two solutions.

The CWM for the problems herein was addressed as a 1-D diffusion from a single (point) reaction site in [Frantziskonis et al, 2006]. For such problems, the coupling of the *fine* and the *coarse* models was done sequentially, i.e. the CWM was used to ensure a robust handshake between the models and the overlap was defined temporally in real time and in real space (not in the wavelet domain). Compounding of information was done temporally in the wavelet domain, and the 1-D wavelet transform was used. When combining the time axis with a spatial one, a 2-D wavelet transform results in 2-D formation of the CWM. This coupling of space and time suggests that the overlap of the *fine* and *coarse* models be defined in the wavelet domain, and this is introduced in this paper. The result is improved spatiotemporal coupling of the two models.

A detailed error analysis and computational efficiency of the CWM studies are presented in section 3. The so-called boundary conditions on the interval are used for the wavelet transform, instead of periodic or fixed boundary conditions. Rigorous use of non-periodic boundary conditions require a threshold value for some of the wavelet coefficients, and is closely tied to stationarity of the signal fluctuations of the in the *fine* model.

1.1 Wavelet Analysis

Wavelets are extremely valuable mathematical tools especially finding uses in the analysis of irregular signals due to their localized nature. Wavelet analysis can be regarded as a mathematical microscope as it enables the examination of broad features of a signal on coarse scales as well as the signal's fine features at fine scales. A brief summary on wavelet transforms appears in the next paragraph for the continuous wavelet transform and in an appendix for the discrete one, while the reader is referred elsewhere for a more comprehensive review [Daubechies, 1992].

In 1-D, a family of wavelet functions $\psi_{a,b}(x)$, can be obtained via dilatations by a scaling factor a, and translations by a factor b of a mother wavelet ψ, and by using this set of wavelet functions, any function $f(x)$ can be transformed as follows:

$$W_f(a,b) = \int_{-\infty}^{\infty} f(x)\psi_{a,b}(x)dx \qquad (1)$$

In particular, for a discrete signal consisting of 2^N data points, N scale decompositions are possible leading to 2^N wavelet transform (WT) coefficients ($W_f(a,b)$). Specifically, the first decomposition yields a set of 2^{N-1} WT coefficients, corresponding to the finest features of the input signal. Next, the second decomposition yields a set of 2^{N-2} coefficients. This process is carried out recursively N times to obtain the complete set of 2^N coefficients. Usually, the final few scale decompositions are represented through the so-called scaling coefficients. The extent of description of the finer features decreases with increasing levels of decompositions, while the exact opposite is true for the coarser features. Further, for the n^{th} scale-decomposition, there are corresponding 2^{N-n} coefficients, out of which, the first and last few coefficients can be of higher magnitude depending on the boundary conditions.

Once the entire spectrum of the WT coefficients $W_f(a,b)$ is obtained, a subset of WT coefficients at any given range of scales between s_1 and s_2 can be used to reconstruct a modified signal $f_{s_1 s_2}(x)$ enabling the examination of the signal at various scales via Eqn. (2a),

$$f_{s_1 s_2}(x) = \frac{1}{c_\psi} \int_{s_1}^{s_2} \int_{-\infty}^{\infty} W_f(a,b) \psi_{a,b}(x) db \frac{da}{a^2} \tag{2a}$$

where c_ψ is a normalization constant. In other words, the inverse wavelet transform can be used as a selective filter, from which a modified signal can be obtained representing the characteristics at some select scales. Note that the original signal can be obtained by using the entire spectrum of scales $(0,\infty)$ in (2a). Extending, one can couple two different signals P_1 and P_2 by identifying the overlapping scales (spatial/temporal) and replacing corresponding wavelet coefficients between the different signals to get a hybrid signal that has the desired characteristics of both signals as shown in the equation below.

$$f_{0,\infty} = \frac{1}{c_\psi} \int_{0}^{s_1} \int_{-\infty}^{\infty} W_f{}^{P_1}(a,b) \psi_{a,b}(x) db \frac{da}{a^2} + \frac{1}{c_\psi} \int_{s_1}^{\infty} \int_{-\infty}^{\infty} W_f{}^{P_2}(a,b) \psi_{a,b}(x) db \frac{da}{a^2} \tag{2b}$$

Although this brief introduction was limited to 1-D WT, WT in 2-D is similar and will be explained in detail later in the paper.

2. Multi-Physics Models at Multiple Scales

2.1 Reaction Dynamics: Kinetic Monte Carlo (KMC)

The *fine* model uses the Kinetic Monte Carlo algorithm for solving the kinetic evolution for the species at the reactive boundary. Uni-molecular reversible first order reactions (3) are considered involving two species, A and B.

$$\begin{aligned} A &\xrightarrow{k_{AB}} B \\ B &\xrightarrow{k_{BA}} A \end{aligned} \tag{3}$$

The rate constants k_{AB}, k_{BA} (each of inverse time (t) units) for the two reactions are taken to be equal to unity (sec^{-1}), while the following are the rate equations for both reactions:

$$\frac{d[A]}{dt} = -k_{AB}[A] + k_{BA}[B], \qquad \frac{d[B]}{dt} = -k_{BA}[B] + k_{AB}[A] \tag{4}$$

The algorithm uses the canonical probability distribution function to describe the probability of the reaction events [Gillespie, 1977], and the time required for one reaction or for a unit change in the concentration of [A], [B] are expressed as

$$\begin{aligned} t_{AB} &= -\frac{1}{k_{AB}[A]}\ln(1-R_1) \\ t_{BA} &= -\frac{1}{k_{BA}[B]}\ln(1-R_2) \end{aligned} \tag{5}$$

where R_1 and R_2 are independent uniformly distributed random numbers between zero and unity.

At any time in the simulation the reaction which requires the least time is the one that will occur. Thus, at every KMC iteration step, two random numbers are generated, *i.e.* R_1, R_2, and t_{AB}, t_{BA} are evaluated based on (5). The minimum of t_{AB}, t_{BA} is the time increment associated with the selected reaction event.

In the KMC formulation no assumption on any statistical dependency among reactive sites is made. The reaction phenomena are equally likely to occur at any of the sites along the boundary at any particular time instant. This is ensured by selecting uncorrelated uniformly distributed random numbers in the KMC. However, two alternate reactions at a specific site (either $A \to B$ or $B \to A$) are

assumed to be perfectly correlated (same random number for each reaction time demand). This is justified from the fact that one of the reactions is fully dependent on the other. Statistically speaking the reaction spatio-temporal field is a white noise field for each individual species (*A* and *B*). However this assumption can be relaxed for situations where a number of different types of independent reactions are possible.

2.2 Reaction Dynamics: Deterministic

The *coarse* model uses a deterministic algorithm for solving the kinetic evolution for the species at the reactive boundary. Equations (4) can be written in a difference form using a first order Eulerian scheme as

$$\Delta[A] = -k_{AB}[A]\Delta t + k_{BA}[B]\Delta t, \qquad \Delta[B] = -k_{BA}[B]\Delta t + k_{AB}[A]\Delta t \tag{6}$$

The difference equations are solved iteratively and the concentrations of [*A*] and [*B*] are updated for each time step.

2.3 Finite Difference Method for Diffusion

Mass transport of the reactive species *A* and *B* are described within the theoretical framework of diffusion, and the relevant equations in two dimensions are written as

$$\begin{aligned} \frac{\partial[A(x)]}{\partial t} &= \left(D_{Ax} \frac{\partial^2[A(x)]}{\partial x^2} + D_{Ay} \frac{\partial^2[A(x)]}{\partial y^2} \right) \\ \frac{\partial[B(x)]}{\partial t} &= \left(D_{Bx} \frac{\partial^2[B(x)]}{\partial x^2} + D_{By} \frac{\partial^2[B(x)]}{\partial y^2} \right) \end{aligned} \tag{7}$$

where D_{pr} denotes the diffusion coefficient of species p (*A* or *B*) along the r^{th} direction (x or y) and all are assumed to be constant and equal to 0.05 in units of space square per unit of time. A finite difference scheme (explicit Euler scheme for time and second order central differencing for space) with fixed time steps Δt and fixed spatial discretization $\Delta x, \Delta y$ are used to solve the above equations. Though higher order schemes can be used, this choice of discretization is sufficient to create a coarse representation.

2.4 The Two Models for 2-D Diffusion with Reactive Boundary

In the two theoretical frameworks, *i.e. fine* and *coarse*, reaction kinetics and mass transport serve as the foundations of a model of a chemically reactive boundary with diffusive species to and from the boundary. The spatially 2-D problem consists of the semi-infinite positive half space (diffusion domain) with chemical reactions taking place at the boundary of the half space (reaction domain). For both theoretical frameworks, the problem of boundary reaction – diffusion is solved by operator splitting [Hairer *et al*, 2002] as described in detail in [Frantziskonis *et al*, 2006]. At the reactive site, concentrations of both A, B are specified by the values evaluated from the reaction kinetics during the operation splitting process.

The boundary conditions considered for the present semi-infinite positive half space field are a) Periodic in the direction of the reactive sites, *i.e.* along the boundary of the half space. b) Reflecting boundary (flux is zero) in the direction transverse to the boundary of the half space. The periodic boundaries are enforced by considering periodic repetition of the nodes *i.e.* the last node in one end will reappear as first node in other extremities. This also enforces flux continuity between the two ends. Reflecting boundary is enforced by making the flux to be zero at the boundary. The updated concentration of species at any other node is calculated by adding contribution of fluxes from all four adjacent nodes. For the reflecting boundary nodes the respective flux in that direction is set to zero. In the present implementation the spatial domains were large enough so that species did not reach the end within the time frame considered.

2.5 Parameters Adopted for Each Model

The problem is defined such that the reaction sites are in the y-direction, at x=0, and diffusion of A and B takes place in the x-y space. Table 1 shows the parameters adopted for each model.

Table 1. Physical parameters adopted for each model

Parameters	*Fine* model	*Coarse* model
Δx: mesh size along x	0.125 units	0.625 units
Δy: mesh size along y	0.125 units	0.125 units
n_x: nodes along x	512	512
n_y: nodes along y	128	128
n_t: no. of time steps	4096	4096
Δt: time step (sec)	$\langle \Delta t_1 \rangle = \frac{0.526}{4096} = 0.0001284$	$\Delta t_2 = 8\Delta t_1, 16\Delta t_1, 32\Delta t_1 \ldots$. etc
T: total run time (sec)	$T1=0.526$	$T2= 4096\,\Delta t_2$
Initial concentrations	A=100 units, B=0 along reactive wall, rest are zero	Same as *fine* model

The parameters in table 1 reflect the difference in various scales involved in the two models. Note that coarse-graining of the KMC reaction sites is not considered at this stage, thus the mesh size along the y-direction is the same for the *fine* and *coarse* models. Thus, in a way, the compounding of the two models presented below is "pseudo" 2-D. Coarse graining at the reaction sites that results in a coarser Δy for the *coarse* model will be presented elsewhere. The time increments in the KMC are not constant since the algorithm finds the minimum time it will take for the next reaction to occur. Thus, $\langle \Delta t_1 \rangle$, *i.e.* the mean value of Δt_1 is shown in table 1. The results presented below are for $\Delta t_2 = 8\Delta t_1$, yet, as shown in table 1, factors larger than 8 have been used for the error analysis presented towards the end of the paper.

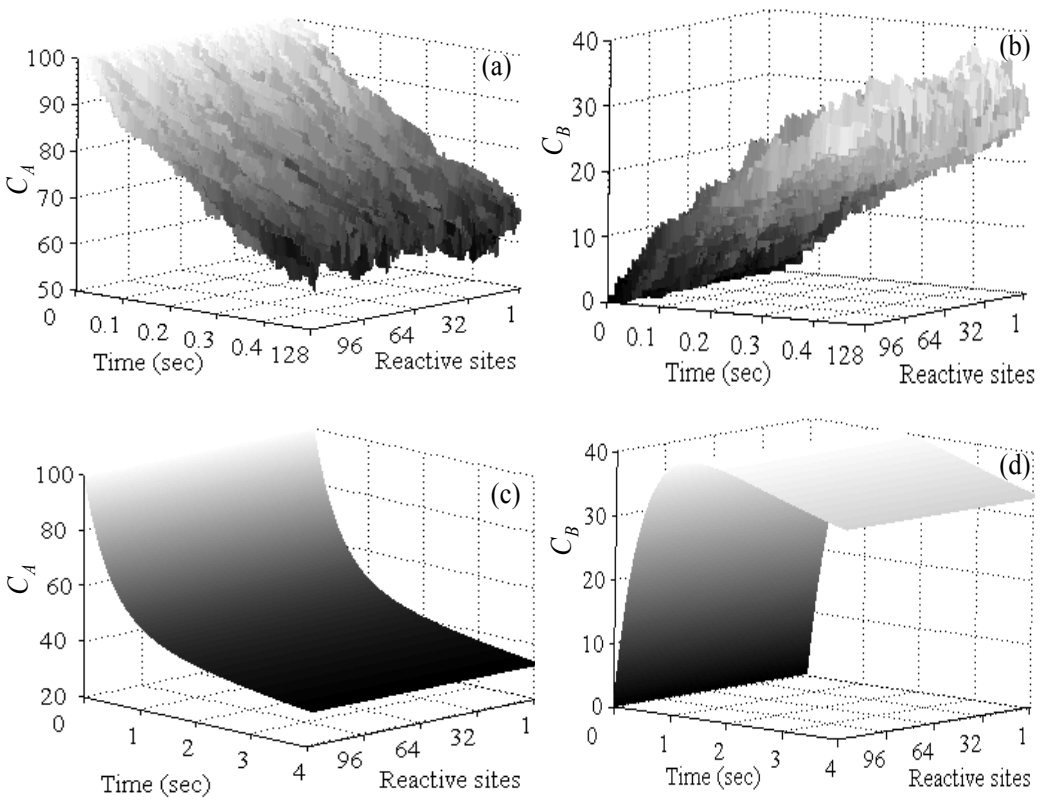

Fig 2 Kinetic evolution of reactants *A*, *B* along reactive (*y* axis at *x*=0) boundary. (a) Concentration of *A*, C_A, from *fine* model; (b) Concentration of *B*, C_B, from *fine* model; Concentration of *A* from *coarse* model; Concentration of *B* from *coarse* model.

2.6 Illustrative Results from the Two Models

Figure 2 shows typical concentrations obtained using the parameters shown in table 1. For the *fine* model, the initially smooth diffusion profile of the evolution is being modified by the fluctuations arising out of the reactive surface. For the *coarse* model, however, the smooth diffusion profile remains smooth due to the absence of fluctuations.

Figure 3 shows the kinetic evolution along the reactive sites (*y* for *x*=0) at several time steps. As can be seen, the fluctuations change with respect to time for the results from the *fine* model, yet this is not the case for the *coarse* model. Since

at the beginning of the simulation (t=0) there are no fluctuations, it is natural that fluctuation increase for certain time period. The statistical analysis of the fluctuations of A and B are examined in detail in a subsequent section.

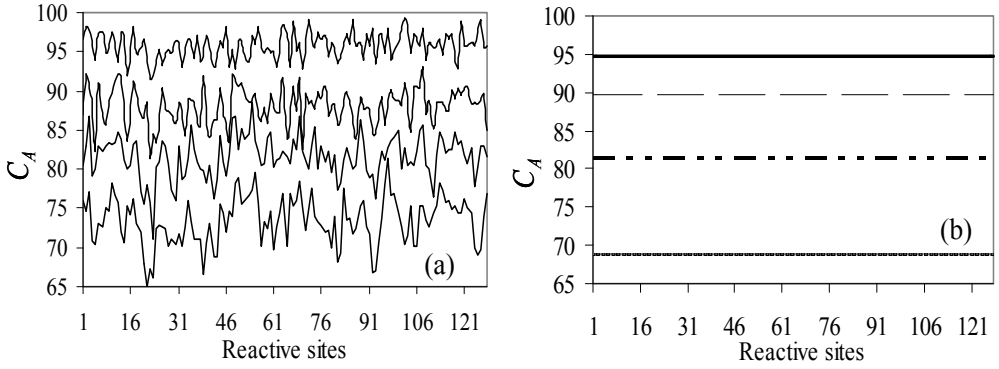

Fig 3 The spatial structure of A along the reactive sites shown as snapshots at several time steps. (a) Fluctuations resulting from the *fine* model. The top curve is at time t=0.025 sec, and at the bottom curve at t=0.4 sec; (b) "Fluctuations" resulting from the *coarse* model. The top curve (solid line) is at time t=0.025 sec, and the bottom curve (short dot line) is taken at t=3.08 sec.

The scale disparity in the two models can be seen more clearly by plotting the concentration of A or B as a function of time for specific reaction sites. Such plots are shown in Fig. 4, for typical reaction sites.

3. Proposed Method for Combining the Multiscale/Multiphysics

3.1 Coupling Scales via the CWM Method

A typical limitation encountered in multiscale simulations that combine two or more different models is the fact that the kinetics driven, high resolution model(s) usually require significantly more number of computations than the models based on integral conservation laws at lower resolution (could extend to several orders of magnitude) in order to model the desired behavior in space and time. CWM strives to overcome this by combining the event driven fine fluctuations that can only be obtained from the high-resolution model with the long-time mean behavior of the integral model(s). As an example, consider two temporal 1-D

signals, one representing the short-time highly accurate trajectory of the system under study - the fine signal, while the other corresponds to an approximate estimate of the mean trajectory of the same system obtained over a much longer time-interval - the coarse signal. Let R denote the ratio of the size of the coarse (Δt_c) and fine (Δt_f) time steps such that $R=2^{n_e}$, while N_c ($=2^{p_c}$) and N_f ($=2^{p_f}$) represent the number of coarse and fine data points, yielding p_c and p_f possible scale decompositions, respectively. Note that by using the coarsest-scale information of the coarse signal in conjunction with Eqn (2b), one can reconstruct the approximate long-time trajectory, while if one uses the coarse-scales of the fine signal only the short-time trajectory is reconstructed. Similarly, using the finest-scales of the fine signal, the fluctuations inherent to the system can be obtained. Thus, information corresponding to two signals differing vastly in the "nature of information" they possess can be coupled together as explained below.

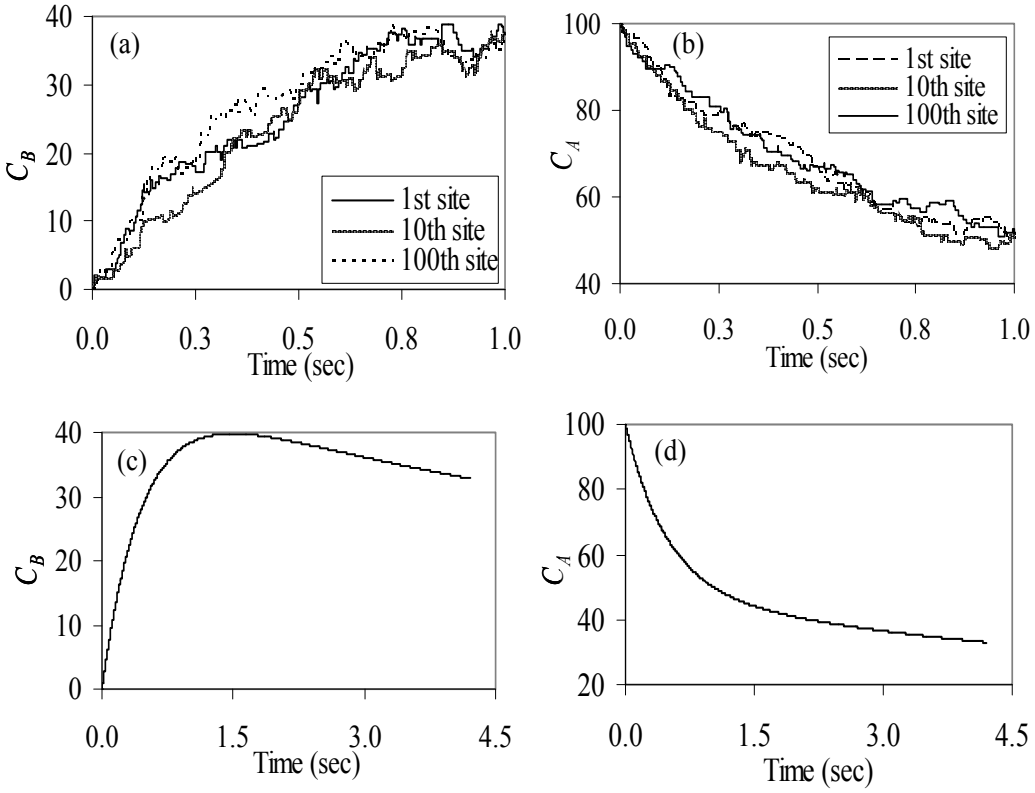

Fig 4 Evolution of reactants *A* and *B* at certain reaction sites resulting from the two models. (a) From *fine* model at 3 reaction sites for *B*; (b) From *fine* model at 3 reaction sites for *A*; (c) From *coarse* model at all reaction sites for *B*; (d) From *coarse* model at all reaction sites for *A*.

Using table 2, where for convenience R, N_c and N_f are chosen to equal 8 (n_e=3), 4096 (p_c=12), and 2048 (p_f=11) respectively, one can identify distinct scale-information corresponding to the two signals, that must be used to obtain the compound wavelet matrix (vector in 1-D). Specifically, using the following series of steps, one can combine information from the two signals in order to obtain the desired compounded signal.

1. Wavelet decomposition: Since the coarsest-scale information of the coarse signal are necessary for reconstructing the long-time mean behavior of the desired signal, WT of the coarse signal are carried out to obtain WT coefficients corresponding to all p_c scales. Similarly, wavelet decompositions of the fine signal are carried out. Correspondence of scales in the two models is deduced from the sampling of the signal at the WT level. Pertaining to that, while p_c and p_f scale-decompositions are possible for the coarse and fine signals, respectively, p_c-3 and p_f-3 scale-decompositions are carried out as shown in Table 2; the reason for this is the correspondence of scales in the two models. The number 3 here is related to the specific scales chosen for the two models. This is further addressed in the following paragraph.

2. Scale selection: As indicated in table 2, an overlap region is first identified and all coarse-signal scales not included in the overlap are selected to represent the coarse-scale coefficients of the compound wavelet vector; the overlap region corresponds to time-scales common to both coarse and fine signals and is determined from the knowledge of p_f and n_e. In this case (*i.e.* in table 2), there are 5 overlapping scales, corresponding to p_f-n_e-3, where "3" represents the number of the finest-scales of the fine signal beyond the overlap, that due to correspondence of scales, they are not included in the formation of the CWM (see discussion on ultra fine scales in a subsequent section). In principle, a larger overlap region leads to a better description of the overall trajectory of the system as more fine-scales of the fine signal can be included in the compounding and if one wants to include all the fine-signal scales, then both signals need to have the same resolution in time.

3. Prolongation: For a given scale, the fine WT coefficients are replicated to ensure consistency in the number of coarse and fine WT coefficients. The number of replications M_p at a given scale is given by $M_p = \frac{N_c R}{N_f}$; in table 2, M_p equals *16*. This replication is a first order approximation at this time as we can assume that the fine scale statistics are stationary and periodic.

4. Thresholding: In order to avoid problems that arise due to the combination of boundary effects and replication of fine WT coefficients, the values of fine WT

coefficients that are greater than a specified cut-off in magnitude are reduced (a detailed discussion is given in a later section, also addressing energy preservation).

5. Replacement: To ensure the preservation of the long-time approximate trajectory of the coarse signal, at every "overlap" scale, any fine coefficient is replaced by its corresponding coarse coefficient if the coarse coefficient is greater in magnitude.

6. Compounding: The selected WT coefficients are assembled to form a compounded matrix (vector in this illustration) that has both coarse and fine WT coefficients.

7. Reconstruction: The hybrid signal is now obtained via Eq. (2b), where both fine and coarse features are included. Note that inversion is not always required or desirable. For example, if statistical information on the signal suffices, the inversion will not provide any additional information, since the statistics can be obtained directly from the CWM.

The above concepts can be readily extended to 2-D; specifically, two-dimensional maps of concentration of species, one axis of the map being time t, and the other axes being the spatial coordinate y are considered. The two-dimensional WT in this case includes transforms in the t direction, the y direction, and in the diagonal t-y direction. The latter is done by constructing wavelet bases from the tensor products of the one-dimensional wavelets in the t and y directions. The details of the wavelet transform, wavelets used, and construction of the CWM in 2-D are given in appendix A, where also details on the boundary conditions used in the wavelet transforms are given; these will prove important when results are presented in the following. For the reader willing to bypass the details and rely on the qualitative issues of the transform, the following example may suffice: given a map (matrix) of dimension 1024x512 in t,y, respectively, the discrete wavelet transform consists of three 512x256 matrices, three 256x128 matrices, and so on; each decomposition level is at half the resolution from the previous one. The final level of decomposition represents the map at the coarsest scale. Once the fine and coarse WT are carried out, appropriate coefficients of the coarse WT matrix are replaced by fine WT coefficients in a fashion analogous to the 1-D case.

Table 2. Schematic coupling of spatiotemporal scales through CWM

Fine Model		Coarse Model			CWM formation	
Wavelet transform	Scale	Wavelet transform	Scale		CWM	CompoundScales
		8	4096 t_{fine}	COARS	8	4096 t_{fine}
		8	4096 t_{fine}		8	4096 t_{fine}
		16	2048 t_{fine}		16	2048 t_{fine}
		32	1024 t_{fine}		32	1024 t_{fine}
8 x 16	256 t_{fine}	64	512 t_{fine}		64	512 t_{fine}
8 x 16	**256 t_{fine}**	**128**	**256 t_{fine}**	COMMON	**128**	**256 t_{fine}**
16 x 16	**128 t_{fine}**	**256**	**128 t_{fine}**		**256**	**128 t_{fine}**
32 x 16	**64 t_{fine}**	**512**	**64 t_{fine}**		**512**	**64 t_{fine}**
64 x 16	**32 t_{fine}**	**1024**	**32 t_{fine}**		**1024**	**32 t_{fine}**
128 x 16	**16 t_{fine}**	**2048**	**16 t_{fine}**		**2048**	**16 t_{fine}**
256 x 16	8 t_{fine}	Tot. 4096	8 t_{fine}	FINE	Tot. 4096	8 t_{fine}
512	4 t_{fine}	t_{fine} ~ time step in Fine model				
1024	2 t_{fine}					
Tot.2048	1 t_{fine}	t_{coarse} ~ time step in coarse model (=8 t_{fine})				

3.2 Compounding – Pseudo 2-D

For the 2-D CWM for the problems herein, the primary scale difference between the *coarse* and *fine* modes is in time *t*. This is because spatial coarse-graining of the reaction sites is not performed, thus the number of reaction sites is the same in the two models. However, the difference in the discretization of the *x*-axis between the two models brings in the effects of spatial scaling. In table 2, a schematic of the compounding technique is shown. This essentially shows the hierarchical decompositions of the concentration maps through the wavelet transform.

By forming the CWM and performing the inverse wavelet transform on it, the multiscale map of concentrations result. Crucial to the success of the method is the number of overlapping scales, in the wavelet domain, between the two

models. Another important factor is the boundary conditions used in the wavelet transform of the map from the *fine* model. The boundary conditions are mainly a reason for considering a threshold value for the wavelet coefficients, as explained in the following sub-section.

3.3 Threshold Value for the Wavelet Coefficients

In wavelet analysis, threshold values are typically used for noise reduction, where wavelet coefficients below a threshold are usually set to zero. The threshold value is generally estimated according to the noise present. There are two types of thresholds reported in the literature namely uniform thresholds and spatially adaptive thresholds. Several algorithms have been proposed for removing additive noise in signal based on thresholds, e.g. [Donoho, 1995]. The threshold value is chosen from estimates of the noise variance.

In the present work, threshold values are used to alleviate problems with the boundary conditions used for the wavelet transform of the maps resulting from the *fine* model. If such maps are periodic, using the periodic boundary condition for the maps does not present any problems and use of threshold values is not needed. However, when this is not the case, use of other boundary conditions such as fixed or even performing the wavelet transform on the interval (see appendix A) results in high wavelet coefficients at and near the boundaries. Even though these coefficients are needed for reconstructing the map by the inverse wavelet transform, they create the following problem when constructing the CWM. For second order statistically stationary maps resulting from the *fine* model, the coefficients at certain scales are repeated in order to match the size of the corresponding matrices in the CWM, and this produces an artificial influence of the wavelet coefficients near the boundary: the number of repetitions M_p amplifies (approximately doubles) the effect of the coefficients near the boundaries. One way to avoid this is to introduce a threshold value and cutoff these boundary coefficients to that value. The value of the threshold can impact the error of the CWM technique.

A simple algorithm to estimate the threshold is used, *i.e.* the value that reproduces the fluctuations of the map as closely as possible, based on statistical energy, is chosen. Since there is interplay between threshold value and number of overlap scales in the CWM, it takes a few iterations until a proper threshold is established. Results presented in the following are for various threshold values.

Figure 5 shows results from the inverse wavelet transform for various values of the threshold and number of overlapping scales. The threshold value used is designated as *T*. Increasing of the threshold and/or the overlap increases

the fluctuations. At large overlap, the impact of threshold on fluctuations diminishes. Figure 5 clearly shows that the replacement step in the CWM ensures the preservation of the long-time coarse behavior. Note that the reconstructed signal exhibits periodicity. The obvious reason is that fine coefficients are periodically repeated to achieve dimensional conformity between equivalent wavelet scales in two models. These repetitions in the wavelet domain show up as periodically repeating peaks in the physical maps. An appropriate value of the threshold diminishes such peaks. However, the possibility of a Kalman filter based Baysian inference technique [Guo et al, 2004] for predicting the unknown fine wavelet coefficients is presently being explored to avoid such repetitions in a more formal way than the thresholding. The other possibility is to reconstruct the signal in real space to the required length preserving the statistics before applying the wavelet transform to avoid boundary edge effects.

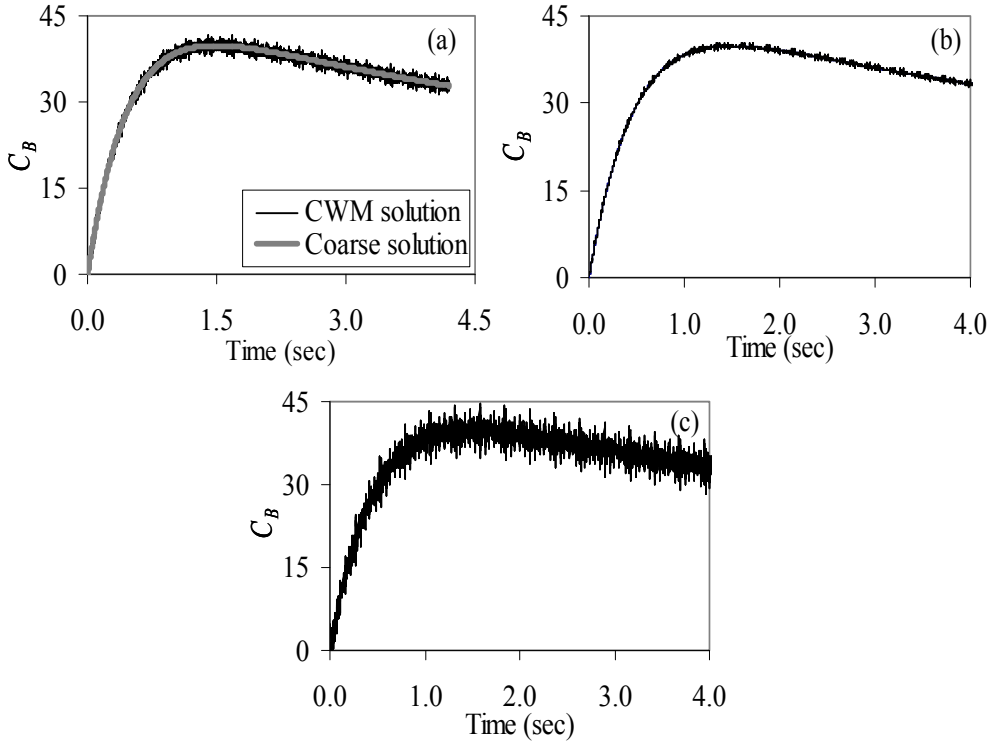

Fig 5 Results from the inverse wavelet transform of the CWM for time evolution of concentration of *B* at the 10th node. (a) *T*=1.0 and 5 overlap scales; (b) *T*=2.0 and 2 overlap scales; (c) *T*=3.0 and 5 overlap scales.

3.4 CWM and Stationarity

The CWM is nicely suited for providing scale-wise statistical information on a problem. For this purpose, performing the inverse wavelet transform of the CWM is not necessary, since the statistics, including correlations along spatiotemporal scales, can be obtained directly from the CWM. However, for certain problems it may by informative to perform the inverse wavelet transform of the CWM and obtain realizations of the problem in actual space and time. In doing so, there is a difference depending on whether the problem (here the reaction-diffusion one) is statistically stationary or not. At certain scales, there will be a mismatch on the number of coefficients provided by the *fine* model and the number of coefficients required by the CWM. Since the mean behavior of the system is obtained from the CWM coefficients provided by the *coarse* model, and the fluctuations from the CWM coefficients provided by the *fine* model, it is important whether the *fine* model provides, or not, results that are second order stationary. If such results are second order stationary, or approximately second order stationary, the coefficients at relevant scales can be repeated in order to fill the CWM out at these scales (due to the properties of the CWM, the number of required repetitions is always an integer). If the fluctuations from the fine model are not stationary, an alternative process can be followed as discussed in the sequence.

For the specific problem studied herein, it will be shown that the assumption of approximately stationary fluctuations is justified if sufficient overlap is assigned between two models. At first glance, it may seem that the fluctuations in the *fine* model tend to increase (see Figs. 1,2) and that would imply non stationarity. This is not the case, however. The change of some statistics with respect to time is presented in Fig. 6. It is apparent that the (first and second order) statistics are changing temporally. The standard deviation increases up to some point and then decreases. The coefficient of variation is quite low, thus, the assumption of the fluctuations being approximately second order stationary appears reasonable. This is addressed further in the error analysis section.

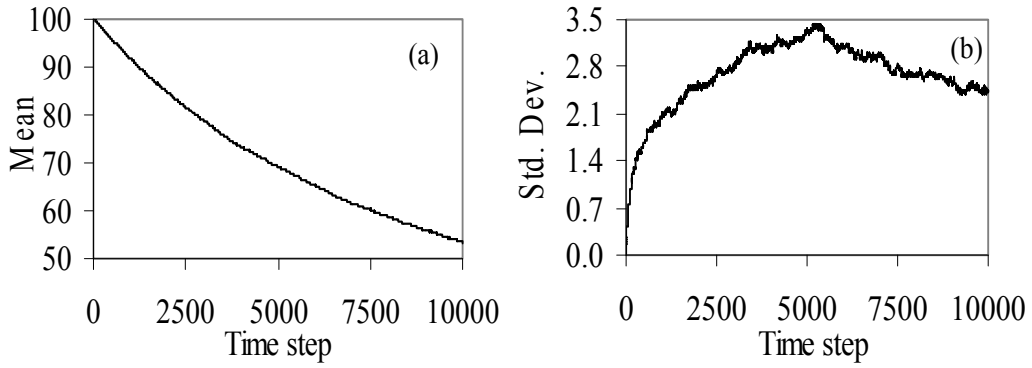

Fig 6 (a) Mean value of concentration of *A* along reactive boundary as a function of time from the *fine* model; (b) Standard deviation of concentration of *A* along reactive boundary as a function of time for the *fine* model.

For the problems examined herein, the following holds: (a) at short times, near the reactive boundary fluctuations are limited since a small number of reactions occur in all sites and thus a smooth concentration profile appears at the reactive sites; (b) also at short times and near the reactive boundary, the concentration-gradient is high because of large concentration of species along the reactive nodes thus the diffusion is rapid, and this can damp out the fluctuations in the concentration profile; (c) at long times, concentrations near as well as far from the reactive sites smooth out due to small concentration gradients which slow down the diffusion and its effect on the fluctuations of the concentration. In order to study the correlation structure of the concentrations, if at all present, concentrations along the reactive boundary are considered. There are three parameters affecting the reproduction of the spatial correlations in CWM: a) the number of overlap scales; b) the threshold value; c) the total time in the simulation. The effect of the overlap in scales was addressed in the previous section where it was shown that the fluctuations increase with increasing overlap. The effect of the other two parameters is examined here, *i.e.* the threshold value and the time. Figure 7 shows typical autocorrelation structures for concentrations along the reactive boundary, *i.e.* plot of

$$\rho(r) = \frac{\langle A(x)A(x+r)\rangle - \mu^2}{\sigma^2} \tag{8}$$

where $\rho(r)$ denotes the autocorrelation as a function of the "lag" r, μ, σ denote the mean value and the standard deviation of species A along the reactive boundary, respectively, and $\langle\cdot\rangle$ denotes expected value. Since at r=0, $\rho(0) = 1.0$,

Fig. 7 shows that the concentrations are practically white noise in the *y*-direction. This conclusion holds for a wide range of the threshold value and for the entire time of the simulation.

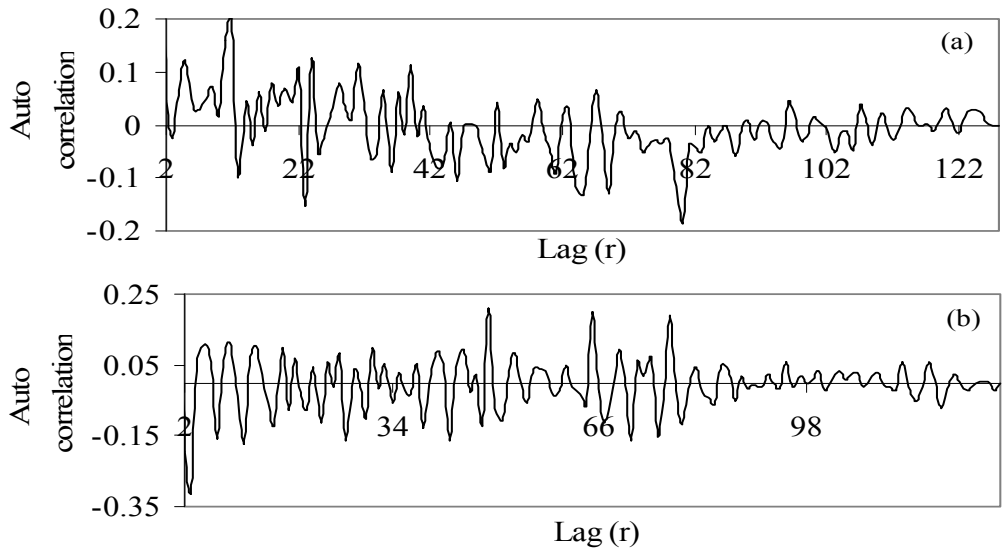

Fig 7 Autocorrelation $\rho(r)$ as a function of *r*, *r*=0,1,2, …, 128 in the *y*-direction, for species *B* at the 500th time step, obtained from (a) the fine model; (b) the CWM method.

3.5 Inclusion of Ultra Fine-scale Data in the CWM and Energy Conservation

In table 2 a schematic of the CWM construction and the available scales from each model is presented. As explained above, ultra fine scales from the *fine* model (sampling interval below $8t_f$) were not included in the construction of the CWM. Due to the mismatch between Δt_c and Δt_f, there is no place (scales) in the CWM where they would be substituted. Since $\Delta t_f << \Delta t_c$, holds, the *fine* model can resolve much finer scales than the *coarse* model. And since the scales from the *coarse* model are used from the beginning of the simulation, the fine scales substitution into the CWM should be limited to those scales which do not exceed the scales of the coarse map. In the present simulations this is satisfied up to the scales with sampling interval $8t_f$. This observation is crucial for maintaining the physical

nature of the compounded map. Any attempts to include those finer scales can result in a distorted map from the inverse transform of the CWM.

There is a way to include all small scales from the *fine* model by resampling the *coarse* model maps at a finer time interval by interpolation. Even though resampling does not add any new information from the *coarse* model into the map, it allows inclusion of ultra fine scales and thus additional information from the *fine* model. One additional important outcome is the process becomes less sensitive to the threshold value. For the present example, the *coarse* model has a time interval of $8t_f$. Resampling results in mathematically equating the scale range of the two maps. Figure 8 shows typical results from this process of resampling the data from the *coarse* model before forming the CWM.

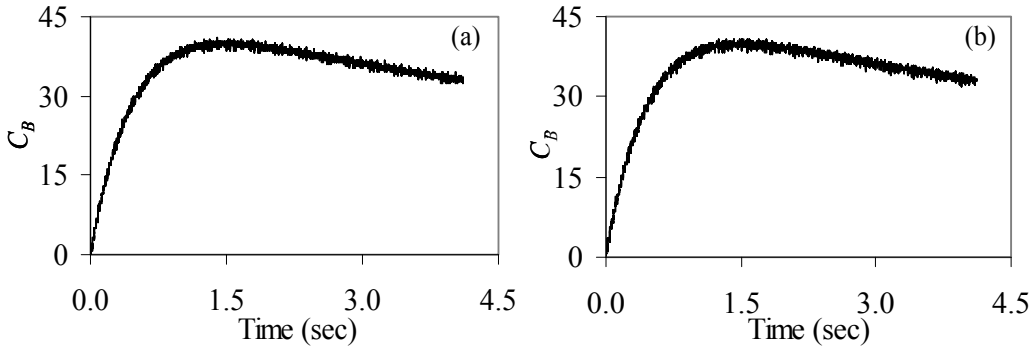

Fig 8 Concentration of B at reactive site 10 obtained by resampling the results from the coarse model before the CWM is constructed. (a) T=2.5; (b) T=5.0.

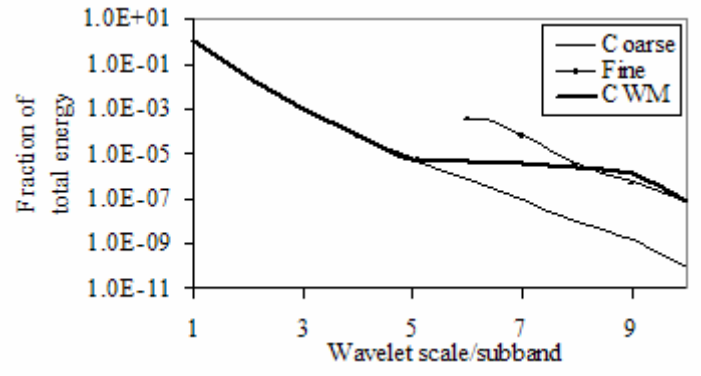

Fig 9 Comparison of energy along scales for the two models and for the CWM maps. The energy axis is logarithmic

It is interesting to observe the energy distribution along scales resulting from the two models and from the compounded maps. Figure 9 shows such a distribution, showing clearly the smooth and natural transition from coarse to fine scales when the CWM is used.

A natural question is about energy conservation in the CWM process. The wavelet transform conserves energy by virtue of the Parseval theorem. This energy is distributed in each wavelet scale, and the distribution is not uniform in general. For the results from the two models herein, the initial few scales (about two for the *coarse* model, more than two in the *fine* model) contain most of the energy, and the contribution from finer scales diminishes progressively along fine scales. This is shown in table 2. The energy contribution decays much faster for the results from the coarse model than those from the fine. This is anticipated due to the fact that *fine* model produces significant information in fine scales. Through CWM these coefficients are transferred to their equivalent scale to impart those fine features. Consequently additional energy is imparted in these scales. Figure 9 shows the individual energy contained in them and redistribution through CWM. However smooth decay/transition of energy from lower to higher subbands/ scales is essential [Wang *et al*,1996, Kadambe, 1992] for maintaining the physical nature of the signal. The M_p repetition of wavelet coefficients if performed without thresholding will increase the energy of the system. Thresholding avoids this by reducing the value of the WT coefficients (near boundaries) that would contribute to this increase.

3.6 Error in CWM Technique with the Overlap Scales

Errors in the CWM solution process include: error in finite difference solution of the diffusion equations (time step, integration method, etc.); error from inappropriate number of overlap scales; error from the boundary conditions used in the wavelet transform and the related threshold value; error in the coarse model in modeling the reactions. This section concentrates in analyzing the error in the CWM technique as compared to the *fine* model acting as benchmark.

If the overlap scales include all the scales available in the *fine* model, then the fluctuations in the CWM will be represented in full detail. Thus, as the number of overlap scales increases, the error decreases, and for sufficient overlap the error should reach a plateau. This plateau value is used here as a reference point, *i.e.* as the benchmark, in order to study the effect of overlap on error. Since the mere time/spatial history does not give a quantitative idea about the intensity of the fluctuations, the L_2 norm of the fluctuations along the reactive boundary as a function of overlap scales n, denoted as $L_{2B}(n)$, is used to study the effect of overlap on error. Figure 10a shows $L_{2B}(n)$ for the A concentrations at the 500^{th} time step, where the asymptotic behavior of the fluctuations with the number of overlap scales can be seen. As the n in $L_{2B}(n)$ increases, the norm approaches saturation. Figure 10b is similar to 10a, yet L_{2B} is normalized with respect to its value at 5 overlap scales, *i.e.*

$$\varepsilon = \varepsilon(n) = \frac{L_{2B}(n_s) - L_{2B}(n)}{L_{2B}(n_s)} \tag{9}$$

where $\varepsilon(n)$ denotes the relative error as a function of the overlap scales n (considering the fluctuations at the saturation number of overlap scales to represent the fluctuations with zero error) and n_s denotes the number of overlap scales at saturation, considered herein equal to 5.

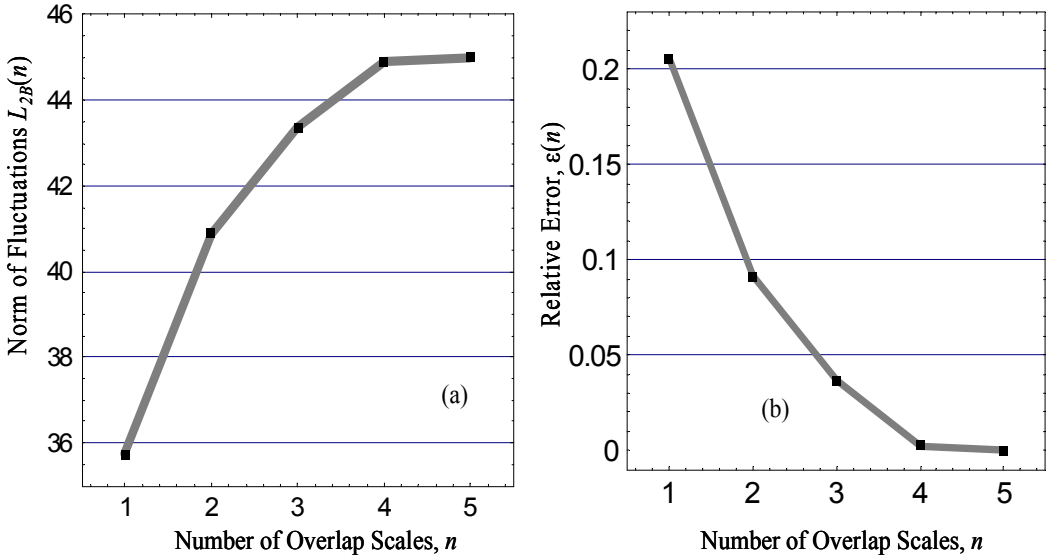

Fig 10 (a) Norm of fluctuations of *A* concentration at the reactive boundary as a function of the number of overlap scales. (b) Relative error as a function of the number of overlap scales.

The error in the solution of the diffusion from a reactive boundary problem is mostly in the diffusion domain, since the KMC and deterministic solution for the reactions are quite accurate and agreeing with each other, *i.e.* the mean response of the KMC is pretty close to the solution of the reactions (3) solved deterministically. It is informative to examine the error from solving the diffusion part of the problem using finite differences. Such a formal examination is presented in appendix II, in 1-D spatial domain for simplicity, where it is shown that

$$Log\left(\varepsilon_f\right) \sim s \tag{10}$$

Holds, where ε_f denotes the relative error in the fundamental solution of the diffusion equation, and s denotes scales in the wavelet transform such that $2^s \sim t$. Superpositions of the fundamental solutions result in the solution of a specific diffusion problem. Figure 11 shows the plot of (10) for the proportionality relation tailored to match the plot in Fig. 10b. As can be seen, the curves in Fig. 10b and Fig. 11 are close to each other, even though the error in the 2-D diffusion problem, including the error in the simulation of the chemical reactions and errors

from the superposition of the fundamental solution, may result in slight alterations of (10).

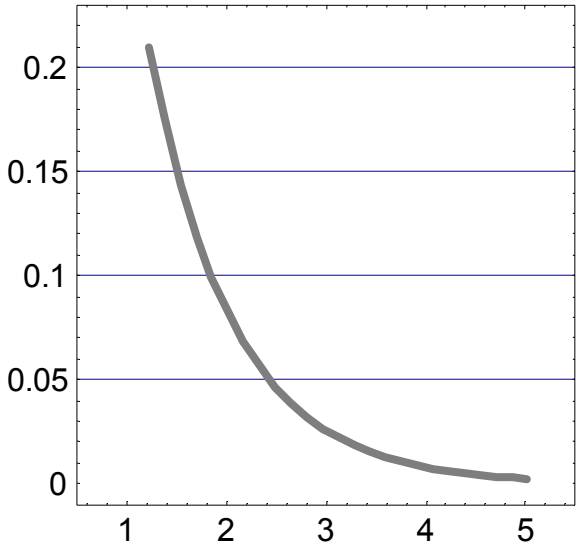

Fig 11 Relative error expressed through equation (10) as a function of scale *s*.

3.7 Error in CWM with Increasing Time Scale Disparity

Another source of error in the CWM process is the difference in time scales involved in the two models. The difference in time scale can be measured by the ratio of the respective time steps. However, as shown from table 3, the number of scales in the overlap domain depends on the ratio of time steps in the two models.

Table 3 The overlapping scales with different time scale ratios.

Equivalent scales are marked by bold letters. First no. is no. of data points and second one is the sampling interval.

Time ratio =8		Time ratio=16		Time ratio=32		Time ratio=64	
Coarse	Fine	Coarse	Fine	Coarse	Fine	Coarse	Fine
4096 (8tf)	2048 (1tf)	4096 (16tf)	2048 (1tf)	4096 (32tf)	2048 (1tf)	4096 (64tf)	2048 (1tf)
2048 (16tf)	1024 (2tf)	**2048 (32tf)**	1024 (2tf)	**2048 (64tf)**	1024 (2tf)	**2048 (128tf)**	1024 (2tf)
1024 (32tf)	512 (4tf)	**1024 (64tf)**	512 (4tf)	**1024 (128tf)**	512 (4tf)	**1024 (256tf)**	512 (4tf)
512 (64tf)	256 (8tf)	**512 (128tf)**	256 (8tf)	**512 (256tf)**	256 (8tf)	512 (512tf)	256 (8tf)
256 (128tf)	**128 (16tf)**	**256 (256tf)**	128 (16tf)	256 (512tf)	128 (16tf)	256 (1024tf)	128 (16tf)
128 (256tf)	**64 (32tf)**	128 (512tf)	**64 (32tf)**	128 (1024tf)	64 (32tf)	128 (2048tf)	64 (32tf)
64 (512tf)	**32 (64tf)**	64 (1024tf)	**32 (64tf)**	64 (2048tf)	**32 (64tf)**	64 (4096tf)	32 (64tf)
32 (1024tf)	**16 (128tf)**	32 (2048tf)	**16 (128tf)**	32 (4096tf)	**16 (128tf)**	32 (8192tf)	**16 (128tf)**
16 (2048tf)	**8 (256tf)**	16 (4096tf)	**8 (256tf)**	16 (8192tf)	**8 (256tf)**	16 (16384tf)	**8 (256tf)**
8 (4096tf)	8 (256tf)	8 (8192tf)	8 (256tf)	8 (16384tf)	8 (256tf)	8 (32768tf)	8 (256tf)

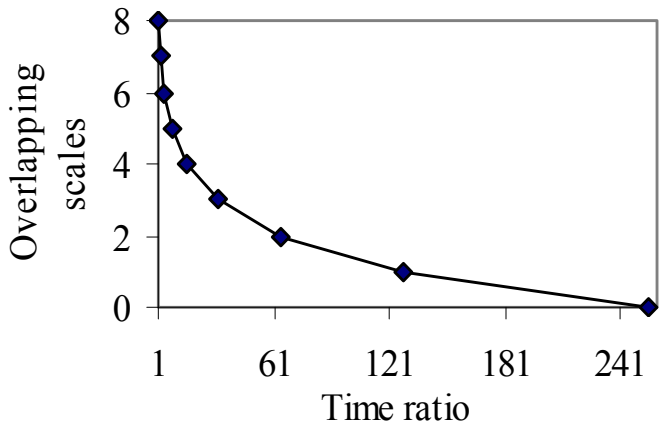

Fig 12 Number of overlap scales available with ratio of time step (coarse to fine)

The plot of the number of overlap scales as a function of the time increment ratio t_c/t_f is shown in Fig. 12. Increasing ratio t_c/t_f implies a decrease in overlap. Therefore the parametric variation of the error will be the same as the one in the previous section.

3.8 Computational Efficiency

A quantitative measure of the computer expense in solving the reaction/diffusion problem using the CWM as compared to a brute force solution method based on the fine model is provided in Table 4. The computer times refer to CPU time on a personal single processor computer operating at 1.8GHz.

Table 4. Comparison of computational expense in the CWM

Model	nx (X-nodes)	ny (Y-nodes)	Kinetic evolution time of the model	computer processing time
Fine	512	128	0.22 sec (2048 steps)	459 sec
			0.41 sec (4096 steps)	948 sec
			3.5520 sec (35520 steps)	8579 sec
Coarse	512	128	3.5144 sec (4096 steps)	928 sec
			1.7572 sec (2048 steps)	515 sec
Wavelet transform				7 sec
CWM	512	128	0.22 sec fine model 3.5144 sec coarse model	7+459+928=1394 sec

For the present problem, it requires much larger CPU time to run the *fine* model for the same evolution time as in the *coarse* model. But the same solution using the CWM requires CPU time that is a little higher than the *coarse* model processing time but much less than the CPU time required by the *fine* model. This is partly due to the fast algorithm for performing the wavelet transform.

The main difference between the *fine* and the *coarse* model is the KMC selection step of the reaction time demand. In each step this includes the generation of random numbers (which requires $O(N)$ operations) and from them calculating the time demand for each site ($O(N)$ operations). These $O(2N)$ operations are part of each step of the kinetic evolution calculations. For the present case the *fine* model requires orders of magnitude more CPU time than the *coarse* model for modeling over the same time interval.

Finally, it is noted that the problems examined herein, no coarse graining of the reaction sites was performed for obtaining the spatial grid of the coarse model. This can increase the efficiency of the CWM substantially and relevant results will be presented elsewhere.

4. Conclusions and Summary

We have presented a detailed example application of the proposed CWM approach for combining information from two physical models (KMC and LBM) that address different spatiotemporal scales. The overlap between the two models is defined in the wavelet domain, and this provides a robust and convenient way to seamlessly link the different physics. An important consequence of our approach is that the computational error can be easily estimated and controlled by changing the degree of scale overlap.

The results presented herein are valid as long as (second order) stationarity is approximately preserved. If this is not the case, longer fine-scale simulations may not be an appropriate alternative even if it is computationally feasible. For problems with non-linearities, stationarity may break down [Muralidharan et al, 2007], and, the CWM method must be made dynamic (DCWM) by restarting the *fine* model simulation as needed to update the statistics prior to compounding. A sequential dynamic coupling is necessary in such cases to catch the system dynamics over a substantial amount of time.

We expect that the basic approach for multi-scale simulation proposed here will be of considerable relevance to chemical reactor engineering research, both in regard to applications and computational simulations. While our CWM method specifically addresses numerical issues, we also believe that the fundamental understanding of the underlying physics can ultimately be improved by the development of better computational models. Thus in the end we hope that both engineering physics and simulation science are served by discussions ensuing from our approach.

NOTATIONS

A chemical species (no. of molecules)

$A(x)$ value of a function at x (unit of x)

$A(x+r)$ value of a function at $(x+r)$ (unit of x)

$[A]$ matrix for forward wavelet transform (dimensionless)

$a(y,t)$ spatial concentration profiles at ordinate a and time t (no./area)

B chemical species (no. of molecules)

C_ψ normalizing constant in inverse wavelet transform (dimensionless)

D_{Ax} diffusion constant of species A in x direction (m/sec^2)

D_{Bx} diffusion constant of species B in x direction (m/sec^2)

D diffusion coefficient for any species (m/sec^2)

$f(x)$ signal defined over space/temporal dimension x (no. of species)

$f_{S_1 S_2}(x)$ wavelet transformed signal f with scale parameter S_1, S_2 (no. of species)

G_i high pass wavelet synthesis filter (dimensionless)

$\tilde{G}_i$ high pass wavelet synthesis filter (dimensionless)

H_i low pass wavelet analysis filter (dimensionless)

$\tilde{H}_i$ low pass wavelet synthesis filter (dimensionless)

h_c coarse discretization of time (sec)

h_f fine discretization of time (sec)

k_{AB} reaction rate constant of A to B reaction (no. of species/sec)

k_{BA} reaction rate constant of B to A reaction (no. of species/sec)

k_c coarse discretization of space (m)

k_f fine discretization of space (m)

$L_2(n)$ $L2$ norm of a signal (square of unit of the signal)

M_p no. of overlapping scales (dimensionless)

n_x no. of grids along x direction (dimensionless)

n_y no. of grids along y direction (dimensionless)

n_t no. of time steps (dimensionless)

N_c no. of data points in coarse solution (dimensionless)

N_f no. of data points in fine solution (dimensionless)

p_f possible no. of scale decompositions in fine solution (dimensionless)

p_c possible no. of scale decompositions in coarse solution (dimensionless)

R ratio of time steps of coarse and fine solution (dimensionless)

$[SYN]$ matrix of backward wavelet transform (dimensionless)

s' scaling coefficients at particular wavelet scale (unit of transformed variables)

t_{AB} reaction time demand for A to B reaction (sec)

t_{BA} reaction time demand for B to A reaction (sec)

T_1 total run time for fine solution (sec)

T_2 total run time for coarse solution (sec)

$W_f(a,b)$ wavelet transform of signal f with scale a and scaled time b (unit of f)

w' wavelet coefficient at particular wavelet scale (unit of transformed variable)

Greek symbols

$\psi_{a,b}(x)$ wavelet basis with scale a and shift b of dimension x (dimensionless)

Δx finite difference grid size in x direction (m)

Δy finite difference grid size in y direction (m)

Δt time steps for reaction-diffusion simulation (sec)

Δt_2 time steps for deterministic reaction-diffusion simulation (sec)

$\langle \Delta t_1 \rangle$ ensembles of time steps of stochastic simulation (sec)

ε_f error in fine solution (no. of species)

$\rho(r)$ spatial autocorrelation function with lag r (unit square of same variable)

Subscripts

$i = \ldots -2, -1, 0, 1, 2 \ldots$ positions of filter coefficients

f parameters associated with fine scale model

c parameters associated with coarse scale model

Superscripts

/ no. of wavelet scale decomposition of the signal

APPENDIX A

A. 1. Illustration of the Wavelet Hierarchical Decomposition of Scales in 2-D and Formation of CWM

This appendix illustrates the wavelet decomposition and CWM formation. In 2-D, one of the dimensions can be space (*x* or *y* axis) and the other time. The *fine* model provides such 2-D maps of concentrations in time-space, *e.g.* a matrix of dimensions 2048x128, the 2048 corresponding to time steps, and the 128 to space discretization in the y-direction. Such a matrix, denoted as *S*, can be decomposed into hierarchy of scales using the wavelet transform. The wavelet transform of a matrix can be performed by pre-multiplying and post-multiplying the matrix by the analyses matrices $[A]^{i}$, $[A]^{ii}$ as

$$\left[WT(S)\right]_{m,n} = \left[A\right]^{i}_{m,m} \left[S\right]_{m,n} \left[A\right]^{ii}_{n,n} \qquad \text{(A.1)}$$

where [*WT*(*S*)] denotes the wavelet transform of [*S*]. The analyses matrices are obtained by forming the block Toeplitz matrix from specific wavelet analysis filter [Harbo and Jensen, 2000]. Typical structure of such block Toeplitz analysis matrix is

$$[A]=\begin{bmatrix} H_0 & H_1 & H_2 & ..... & & .... & H_{-2} & H_{-1} \\ G_0 & G_1 & G_2 & ..... & & ..... & G_{-2} & G_{-1} \\ H_{-2} & H_{-1} & H_0 & H_1 & H_2 & ..... & & ..... \\ G_{-2} & G_{-1} & G_0 & G_1 & G_2 & .. & & .. \\ & ... & H_{-2} & H_{-1} & H_0 & H_1 & H_2 & ... \\ & .... & G_{-2} & G_{-1} & G_0 & G_1 & G_2 & ... \\ H_2 & .... & .... & H_{-3} & H_{-2} & H_{-1} & H_0 & H_1 \\ G_2 & .... & .... & .... & G_{-2} & G_{-1} & G_0 & G_1 \end{bmatrix} \quad \text{(A.2)}$$

Here *H* and *G* denote the High and Low pass wavelet filters respectively. The filter coefficients are wrapped around the boundary, typically the case for analyzing periodic problems. For a finite signal however one need to use the wavelet transform in the interval. For that case, special boundary filters replace the end couple of rows with no periodic wrapping. The details of such implementation can be found in [Harbo and Jensen, 2000].

Once the signal is multiplied by the analysis matrix then a down sampling operation is performed which groups the low pass part in the upper half and high pass part in the lower half of the matrix. Mathematically,

$$SC(i,j)=S((2i-1),(2j-1)); \quad WV(n/2+i,n/2+j)=S(2i,2j)$$
$$(i,j=1,2,...,N/2) \quad \text{(A.3)}$$

where *SC* and *WV* are the upper and lower part of the wavelet transform map *S* at a particular scale. The same operations are then repeatedly performed on the scaling coefficients at each scale to achieve progressively lower resolution at progressively lower scales; the final matrix is the so-called scaling coefficient matrix. The whole algorithm is performed with a fast algorithm. The whole structure of the algorithm is shown in (A.4)

$$\begin{Bmatrix} S_1 \\ S_2 \\ S_3 \\ S_4 \\ S_5 \\ S_6 \\ S_7 \\ S_8 \end{Bmatrix} \rightarrow \begin{Bmatrix} s_1^{'} \\ s_3^{'} \\ s_5^{'} \\ \hline s_7^{'} \\ w_2^{'} \\ w_4^{'} \\ w_6^{'} \\ w_8^{'} \end{Bmatrix} \rightarrow \begin{Bmatrix} s_1^{''} \\ s_5^{''} \\ \hline w_3^{''} \\ w_7^{''} \\ \hline w_2^{'} \\ w_4^{'} \\ w_6^{'} \\ w_8^{'} \end{Bmatrix} \qquad \text{(A.4)}$$

where the first vector is the actual signal. The arrow sign implies multiplication by the analysis matrix and down sampling. Thus scaling and wavelet coefficients are obtained for that scale. For the next scale once again the scaling coefficients of the present scale is multiplied by analysis matrix and down sampling will give the scaling and wavelet coefficients of the next higher scale and so on.

The backward or inverse wavelet transform is performed to regain back the original signal from the wavelet coefficients obtained by forward transform. This is done by first performing the up-sampling operation on the scaling and wavelet coefficients. Mathematically the up-sampling is expressed as

$$S(2i-1,2j-1) = SC(i,j); \qquad S(2i,2j) = WV(i,j) \quad (i,j=1,2,...,N/2) \qquad \text{(A.5)}$$

After that, the up-sampled vector is multiplied by the synthesis matrix. Like the analysis matrix the synthesis matrix is also another block Toeplitz matrix formed as

$$[SYN] = \begin{bmatrix} H_0 & H_1 & H_2 & ..... & & .... & H_{-2} & H_{-1} \\ G_0 & G_1 & & ..... & & ..... & G_{-2} & G_{-1} \\ H_{-2} & H_{-1} & H_0 & H_1 & H_2 & ..... & & ..... \\ G_{-2} & G_{-1} & G_0 & G_1 & G_2 & .. & & .. \\ & ... & H_{-2} & H_{-1} & H_0 & H_1 & H_2 & ... \\ & .... & G_{-2} & G_{-1} & G_0 & G_1 & G_2 & ... \\ H_2 & .... & .... & H_{-3} & H_{-2} & H_{-1} & H_0 & H_1 \\ G_2 & .... & .... & .... & G_{-2} & G_{-1} & G_0 & G_1 \end{bmatrix} \qquad \text{(A.6)}$$

The structure of the synthesis matrix is similar to that of the analysis matrix except the filters. The high and low pass synthesis filters are not independent of each other they are related by the following relations for bi-orthogonal (used in this paper) filter.

$$\tilde{G}(n) = (-1)^n H(1-n) \quad \text{and} \quad g(n) = (-1)^n \tilde{h}(1-n) \tag{A.7}$$

The choice of the wavelet family is important for each specific problem. For preserving the symmetry and physical appearance of a problem, without totally sacrificing orthogonality, symmetric biorthogonal filters provide a great choice. Also for exact treatment of the boundary the so-called biorthogonal CDF(4,6) wavelet is used herein with boundary corrections in the interval. Detailed implementation of the CDF family is provided by [Harbo & Jensen, 2000].

Using the discrete wavelet transform a 2-D map is transformed into various scales as shown in Fig. A1. The matrix of size 2048x128 (kinetic evolution map) is decomposed into a series of scales. A matrix similar to Fig. A.1 results from both the *fine* and *coarse* models.

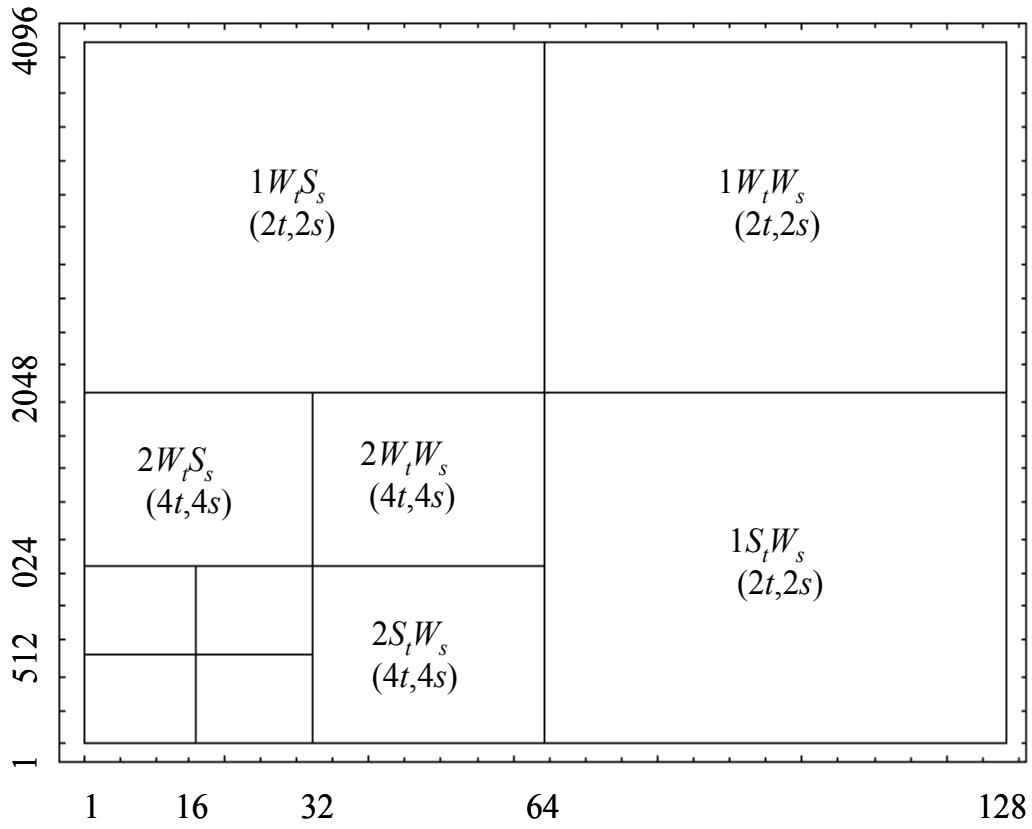

Fig A.1 Wavelet decomposition of fine model. 5 scales (4 wavelet, 1 scaling) are used in the wavelet decomposition. Notation: *W*- wavelet transform coefficients; S - scaling coefficients; t – time variable; s - space variable; the number in each box refers to the scale number. The sub matrices dimensions can be deduced from the horizontal and vertical axes.

A.2 CWM Formation through Compounding

Once the multi scale decompositions are available from the *fine* and *coarse* models, these are then compounded to form the CWM. In forming the CWM the higher scales decompositions are those of the *fine* model. Of course, there may be dimensional mismatch, i.e. although the scales of the *fine* model and the CWM are matched, the size of the matrices in the *WT* of the *fine* model can be smaller than those in the CWM. For the purpose of extracting statistical information, this mismatch does not pose any problems. However, if the inverse wavelet transform

of the CWM is to be performed, then the mismatch needs to be addressed. For periodic boundary conditions in the *fine* model, periodic repetitions of the submatrices from the WT of results from the *fine* model fill out the corresponding CWM submatrices. The same holds when the results from the *fine* model are second order stationary, since the trend of the response is obtained from the *coarse* model. For cases where the results from the *fine* model are not second order or approximately second order stationary, the CWM must be constructed for relatively small time intervals, and the process is repeated in time (a number of CWMs are formed) as mentioned in the "Conclusions and Future Issues" section. The information on coarse scales is taken form the *coarse* model. The equivalency of scales in the WT of the fine, coarse model and those in the CWM can be determined by merely observing their sampling interval.

The scales common to both models forms the overlap. As the scale difference between the two models increases, the number of overlapping scales decreases. For the problems addressed herein, even one scale overlap may be sufficient to obtain reasonable results (with little error). However this may vary depending upon the problem being studied. Table A.1 shows the overlap scales as well as the equivalent scales for various values of the ratio of time increments (t_{coarse}/t_{fine}) and corresponding ratio of space discretization (s_{coarse}/s_{fine}). It is not necessary that (t_{coarse}/t_{fine})= (s_{coarse}/s_{fine}), yet the cases shown in the table facilitate understanding of overlap and equivalent scales.

Table A.1 Equivalent scales for forming CWM

Time ratio: (t_{coarse}/t_{fine}) Space ratio: (s_{coarse}/s_{fine})	Overlap scales	Equivalent scales	Match dimension of scale from fine model to CWM
2 (t_{coarse} =2 t_{fine}) (s_{coarse} =2 s_{fine})	Coarse (1,2,3) Fine (2,3,4)	1st Coarse - 2nd Fine 2nd Coarse - 3rd Fine 3rd Coarse - 4th Fine	4 times repetition of fine sub matrices are required in both directions
4 (t_{coarse} =4 t_{fine}) (s_{coarse} =4 s_{fine})	Coarse (1,2) Fine (3,4)	1st Coarse - 3rd Fine 2nd Coarse - 4th Fine	8 times repetition
8 (t_{coarse} =8 t_{fine}) (s_{coarse} =8 s_{fine})	Coarse (1) Fine (4)	1st Coarse - 4th Fine	16 times repetitions
16 (t_{coarse} =16 t_{fine}) (s_{coarse} =16 s_{fine})	No overlap		

APPENDIX B

The diffusion equation in one spatial dimension, *i.e.* diffusion in y

$$\frac{\partial[a(y,t)]}{\partial t} = D\frac{\partial^2 a(y,t)}{\partial x^2} \tag{B.1}$$

where $a(y,t)$ denotes the concentration of diffusing species a at coordinate y and time t, and D denotes the diffusion coefficient, can be solved numerically by discretizing y in intervals of length h and time in intervals of time k. The error from a forward difference (explicit) finite difference solution is expressed as [*e.g.* Duchateau & Zachmann, 1986]

$$error \sim \frac{k}{2}\frac{\partial^2 a(y,t)}{\partial t^2} - D\frac{h^2}{12}\frac{\partial^4 a(y,t)}{\partial x^4} = O\left(k + h^2\right) \tag{B.2}$$

The fundamental solution (Green's function) to (B.1) reads

$$a(y,t) = \frac{1}{2\sqrt{D\pi t}} \exp\left(-\frac{y^2}{4Dt} \right) \tag{B.3}$$

For the fundamental solution (B.3), a straightforward evaluation shows that the *error* (B.2) is maximum at y=0, and at that spatial coordinate, the error is expressed as

$$error = \frac{k\left(6r-1\right)}{32\sqrt{D\pi} r t^{5/2}} \tag{B.4}$$

where

$$r = D\frac{k}{h^2} \tag{B.5}$$

Note that the error in (B.4) tends to zero at r=1/6, which implies a time increment equal to 1/3 of the time increment at the numerical stability limit. At that specific value of r, the error becomes $O\left(k^2 + h^4\right)$ [Duchateau & Zachmann, 1986]. Yet, for the purposes herein we consider $r \neq 1/6$ (and r relatively far from 1/6) and thus error of $O\left(k + h^2\right)$).

Let ε_f denote the relative error in the fundamental solution, *i.e.*

$$\varepsilon_f = \frac{error_c - error_f}{\dfrac{1}{2\sqrt{D\pi t}}} \tag{B.6}$$

where $error_c, error_f$ denote the error in the *coarse* and *fine* model, respectively, and the denominator in (B.6) is simply the fundamental solution evaluated at y=0. Denoting by k_c, k_f the time discretization in the *coarse* and *fine* models, and by h_c, h_f the corresponding space discretization, respectively, and setting for simplicity

$$r = D\frac{k_c}{h_c^2} = D\frac{k_f}{h_f^2} \tag{B.7}$$

it follows that

$$\varepsilon_f = \frac{\left(k_c + k_f\right)\left(6r-1\right)}{8rt} \tag{B.8}$$

Considering that $k_c >> k_f$, the relative error in the fundamental solution is proportional to the time discretization in the coarse model. Since the scales, *s*, in the wavelet transform are such that $2^s \sim t$, and since k_c and *t* are directly related to the overlap scales in the CWM method, it follows that

$$Log\left(\varepsilon_f\right) \sim s \tag{B.9}$$

REFERENCES

Breault, R., "A Review of Gas-Solid Dispersion and Mass Transfer Coefficient Correlations in Circulating Fluidized Beds", Powder Technology, Vol. 163, 9-17 (2006).

Daubechies, I., "Ten Lectures on Wavelets," Society for Industrial and Applied Mathematics (SIAM), Philadelphia, Pennsylvania (1992).

Donoho, D., L., "De-noising by soft Thresholding", IEEE Transactions on Information Theory, Vol. 41, 613-627 (1995).

Duchateau, P., Zachmann, D.,W., "Partial Differential Equations," McGraw-Hill, New York (1986).

Frantziskonis, G., Mishra, S., K., Pannala, S., Simunovic, S., Daw, C., S., Nukala, P., Fox, R., O., Deymier, P., A., "Wavelet-based Spatiotemporal Multiscaling in Diffusion Problems with Chemically Reactive Boundary", International Journal of Multiscale Computational Engineering, Vol. 4, 755-770 (2006).

Gillespie, D., T., "Exact Stochastic Simulation of Coupled Chemical Reactions" Journal of Physical Chemistry, Vol. 81, 2340-2361(1977).

Guo, D., Wang, X., Chen, R., ''Wavelet-Based Sequential Monte Carlo Blind Receivers in Fading Channels With Unknown Channel Statistics'', IEEE Transactions on Signal Processing, Vol. 52, 227- 239 (2004).

Hairer, E., Lubich, C., Wanner, G., "Numerical Integration: Structure Preserving Algorithms for Ordinary Differential Equations," Springer Verlag, Berlin (2002).

Harbo-Cour, A., and Jensen, A., "Ripples in Mathematics The Discrete Wavelet Transform," Springer (2000).

Hill, R., J., Koch, D., L., Ladd, A., J., C., "The first effects of fluid inertia on flow in ordered and random arrays of spheres," Journal of Fluid Mechanics, Vol. 448, 213-241 (2001a).

Hill, R., J., Koch, D., L., and Ladd, A., J., C., "Moderate-Reynolds-number flows in ordered and random arrays of spheres," Journal of Fluid Mechanics, Vol. 448, 243-278 (2001b).

Kadambe, S., "On the Choice of a Wavelet, and the Energy and the Phase Distributions of the Wavelet Transform", Time-Frequency and Time-Scale Analysis, Proceedings of the IEEE-SP International Symposium, Vol. 4-6, 379-382 (1992).

Succi, S., Filippova, O., Smith, G., Kaxiras, E., "Applying the Lattice Boltzmann Equation to Multiscale Fluid Problems," Computing in Science and Engineering, Vol. 3, 26-37 (2001).

Vanderhoef, M., A., Beetstra, R., and Kuipers, J., A., M., "Lattice Boltzmann simulations of low Reynolds number flow past mono- and bi-disperse arrays of spheres: results for the permeability and drag forces," Journal of Fluid Mechanics, Vol. 528, 233-254 (2005).

Wang, X., Wu, G., Lin. X., "Image Coding Based on Energy Estimation and Reordering of Wavelets," Proceedings of the 34d International Conference on Signal Processing, Beijing, China, 295-298(1996).